3D MONITORING OF COASTAL EROSION CONTROL STRUCTURES USING UAV

N. Sakamoto[1], S. Nishiyama[1]

[1] Graduate School of Environmental and Life Science, Okayama University, Okayama city, Japan – p9ly7aer@s.okayama-u.ac.jp, nishiyama.satoshi@okayama-u.ac.jp

KEY WORDS: Laser surveying, Green laser drone, 3D point cloud, Coastal erosion control, ICP.

ABSTRACT:

Coastal erosion has increasingly become a problem in recent years due to rising sea levels caused by global warming. To prevent further coastal erosion and damage, control structures like seawalls and breakwaters have been installed along vulnerable coastlines. However, it is crucial that these structures are regularly and thoroughly inspected for any abnormalities or deformations. At present, inspections are done manually by visual surveys which are time-consuming and inefficient. There is great potential to optimize this process using drone technology equipped with 3D laser scanners. In this study, we utilized a drone with a green laser scanner to inspect and diagnose control structures along the coast. We conducted surveys to determine the basic performance of this approach and used ICP algorithms to extract any deformations in vanishing wave blocks over two time periods. Our results showed high variability in basic performance due to the influence of waves during the surveys. However, we were still able to detect strain of around 50 cm in a submerged breakwater located 3 meters below the water's surface. Furthermore, an overall settlement of approximately 34 cm was observed in the vanishing wave blocks along with some localized movements. This demonstrates that drones can be successfully implemented for efficient inspection, diagnosis and detection of abnormalities and deformations in coastal structures that are extremely difficult to identify through visual surveys alone. The use of this advanced technology will allow for quicker identification of at-risk structures, enabling timely maintenance and prevention of further coastal erosion.

1. INTRODUCTION

1.1 General Instructions

Japan, an island nation, has approximately 34,000-km coastline, which is significantly longer per unit area of land compared to other countries. Coastal areas are prone to disasters, and in Japan coastal erosion is a significant problem. It has been exacerbated by factors such as rising sea levels due to global warming. As a result, approximately 160 hectares of land are lost annually, making the efficient inspection of coastal protection facilities a critical issue. To address this, coastal erosion countermeasures such as breakwaters and artificial reefs have been installed nationwide. To assess the condition and effectiveness of these structures, it is essential to efficiently understand the shape and condition of the seabed and coastal structures.

Currently, visual inspections are the primary method used; however, with the recent push for construction digitalization, there is a demand for more efficient, unmanned, and labour-saving inspection methods. Narrow multibeam acoustic depth measurement and airborne laser depth measurement are used for monitoring underwater structures that cannot be visually inspected. However, there are challenges in terms of measurement difficulties in certain locations and cost considerations. In this study, we conducted surveys with drones equipped with a green laser scanner that penetrates underwater to understand the basic performance and identify the changes in wave-dissipating blocks (tetrapods) over two periods using the iterative closest point (ICP) method. The study aims to discuss the methods used and future challenge.

2. SURVEYING METHODS FOR SEAFLOOR TOPOGRAPHY

2.1 Existing methods for seafloor topography measurement

Among the existing methods for underwater terrain surveying, two representative methods are narrow multibeam acoustic sounding and airborne laser bathymetry (ALB).

2.1.1 Narrow multibeam acoustic sounding: Narrow multibeam acoustic sounding uses a ship to transmit sound waves from a sonar head and receive reflected waves from the seabed, calculating distance from the speed, distance and time relation and relying on three-dimensional data of the reflection from surfaces. As a feature, it is the most widely used method for measuring seabed terrain because it can measure deep sea terrain with water depths up to 7000 meters. However, it is limited in very shallow coastal environments and areas inaccessible to survey ships, such as rocky reefs, due to constraints like acoustic interference and minimum slant range requirements. Advances in transducer design allow multibeam systems to achieve wide swath widths up to 10 times the water depth and high spatial resolution on the order of a few percent of depth. Still, complementary techniques like airborne lidar bathymetry may be required for complete high-resolution coverage in extremely shallow nearshore zones.

2.1.2 Depth measurement by ALB: Depth measurement by airborne laser bathymetry (ALB) utilizes near-infrared lasers reflected off the water surface and green lasers that penetrate into the water column. Water depth is calculated from the difference in two-way travel time between these laser returns. This light detection and ranging (lidar) approach allows measurement of shallow waters and nearshore areas inaccessible to survey ships and crews. However, low-cost, high density point cloud coverage over large areas can be challenging to achieve with aerial platforms. Ongoing technological advances aim to improve laser repetition rates, positioning, and scanning mechanisms to increase depth measurement density and spatial coverage. Still, seafloor reflectivity, water clarity, and surface conditions impact ALB penetration depth and accuracy. Multisensory fusion with acoustic sounding data helps supplement ALB and expand its capabilities for mapping coastal bathymetry at high resolution.

2.2 An Overview of Drone Equipped with Green Laser Scanner

In this study, measurements were carried out using a drone equipped with a green laser scanner. Drone surveying with a green laser scanner (hereafter, drone surveying) involves mounting a lightweight green laser scanner on a nimble drone and irradiating green lasers from the air to survey land and water areas simultaneously. The green laser is modulated laser light with a wavelength of around 800nm emitted from a diode and has the characteristic of penetrating water. Therefore, it is possible to extensively and seamlessly survey the underwater terrain of shallow waters and ground surfaces that are not yet fully dried. While airborne laser bathymetry (ALB) using green lasers is common for measuring seabed topography, it is difficult to conduct rapid, low-cost measurements, and the required altitude over 400m makes acquiring high-density point cloud data challenging. In contrast, with drone surveying, lowering the measurement altitude to under 150m enables acquisition of high density point clouds exceeding 100 points/m2. Thus, this new technique shows promise for understanding coastal zone topographical changes near water's edge, seafloor morphology in surf zones, and structural shapes (Tomii, 2021). The equipment used for the measurements is shown in Figure 1. The specifications of the green laser scanner used in this study are as follows: Dimensions (with propellers, frame arms, GPS mount deployed and landing gear): 1688mm×1518mm×727mm; Weight: 10kg; Maximum speed: 40km/h, 65km/h (no wind); Operational altitude limit (above sea level): 2500m; Size: 280mm×140mm×210mm; Laser wavelength: 532±1nm; Maximum measurement distance: ≧10% 158m/ ≧60% 300m over; Accuracy: ≧10% ±15mm/ ≧60% ±5mm; Laser irradiation angle: 30 degrees; Pulse rate: 60kHz/s; Scan speed: 30 scans/s; Beam divergence angle: 1.0mrad.

During drone surveying, self-positioning relies on GNSS (Global Navigation Satellite System) reception, which can be affected by the reception environment. Thus, depending on the time and location of surveying, high precision measurements may not be achievable. Additionally, the greater the laser scan angle deviation from vertical, the more drone attitude affects measurement accuracy. IMUs (Inertial Measurement Units) measure and control pitch, roll, and acceleration in 3 axes (X, Y, Z) to determine drone attitude during flight.

Challenges for drone surveying include limited flight times when heavier laser scanners are mounted on drones due to battery life restrictions, making wide area monitoring in short time periods difficult. To address this, development of lighter laser scanners and engines to enable longer drone flights is underway.

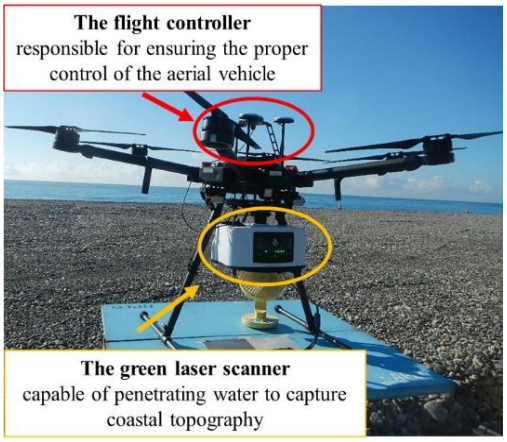

Figure 1. Drone equipped with a green laser scanner.

2.3 Measurement Overview

In this chapter, we provide an overview of the measurements conducted and the subjects of measurement in this study, along with a summary of the results.

2.3.1 Survey implementation overview: The measurement site is a part of Shichiri Mihama Beach, which stretches approximately 22 km from Kumano City to Kiho Town in Mie Prefecture. The site is shown in the photograph in Figure 2 above. The measurement area stretches approximately 400 m along the coast and extends 300m offshore, the area is highlighted by a red frame in Figure 2. The measurements were conducted in two periods, with the first period on July 20, 2021, and the second period on November 24, 2021. The drone flight time was approximately 1 hour and 20 minutes for both periods, with a flight altitude of 60m, a flight speed of 3m/s, with a side overlap rate of 28%. In addition, the square and triangle shown in the figure indicate the positions of the control points and verification points, respectively, where the adjustment of point cloud positions and verification of point cloud acquisition accuracy were performed.

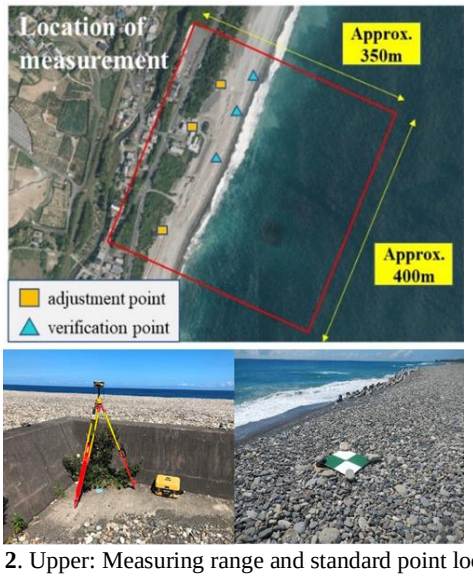

Figure 2. Upper: Measuring range and standard point location. Lower left: GNSS Receiver at the Base Station, Lower right: Exterior View of the Verification Point.

2.3.2 Land-based accuracy verification: Three adjustment points and validation points were set within the measurement range. Using these reference points, accuracy verification was conducted by comparing coordinates obtained through GNSS surveys. Figure 2 below illustrates the diagram of fixed stations and validation points. As it was not feasible to install reference points underwater, the accuracy verification was confined to land-based areas. However, validating the accuracy of land-based acquisitions is crucial for handling three-dimensional data in the coastal zone, even though it excludes underwater accuracy assessment. Mean and standard deviation of survey errors were computed for both the first and second periods. Errors concerning adjustment points consistently remained below ±50mm, with a maximum standard deviation of 0.35mm in both periods, indicating the capability to obtain point cloud data of sufficiently high accuracy even without adjustment points. Regarding validation points, the first period displayed a standard deviation of approximately 10mm, while the second period showed approximately 30mm, both falling below the acceptable error margin of ±50mm. Nevertheless, in coastal measurements, having only three adjustment points along the coastline and the inability to establish such points underwater pose challenges for the spatial alignment of point cloud data. Furthermore, since underwater accuracy verification is unfeasible, there arises a necessity to explore methods for validating the accuracy of point cloud data acquired underwater in future endeavours.

3. RESULTS

3.1 Surveying Results

A contour map of point cloud data obtained by surveying is shown in Figure 3. It can be seen from the variation in the blue area that the terrain has changed significantly over approximately four months. At the observation site in Shichiri Mihama, Mie Prefecture, rainfall continued for ten days from August 11 to 21, 2021, and on August 17, heavy rain of about 120 mm per hour was observed in Mie Prefecture. These events occurred between the first and second surveys, and the coastal terrain was significantly altered due to their effects. From the data of the second survey, it was also confirmed that the erosion of the coast was suppressed by the wave-dissipating blocks installed on the coast. This indicates that coastal erosion prevention measures are effective. In addition, in the accuracy verification of drone surveying using adjustment points and verification points, the point acquisition accuracy on land was less than ±50mm for both adjustment and verification points, indicating good accuracy.

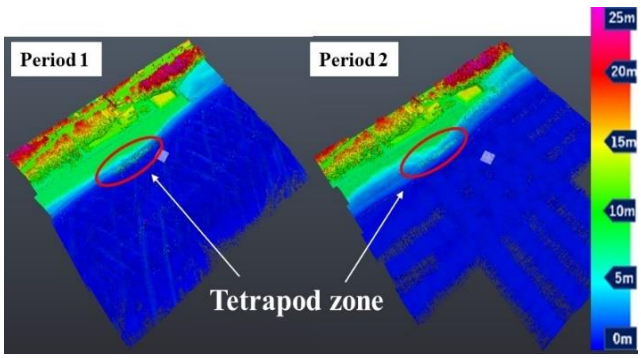

Figure 3. Left: Measurement result of the first period, Right: Measurement result of the second period.

3.2 Point Cloud Data Analysis

3.2.1 Cross section extraction: The diagrams in figure 4 show the extraction positions and cross-sectional views for the first and second time periods. The cross-sections of the same location in both periods are shown. The upper diagram represents the extracted location and the cross-section from the first period, while the lower diagram represents them from the second period. In the cross-section, the green point cloud represents data from the land area, while the turquoise point cloud indicates data from the sea surface. However, during the initial survey period, no point cloud data from the seabed could be obtained, leading to an inability to identify the sea surface data. Consequently, coloration was applied based on orthoimages.

In the first survey period, as described above, seafloor point cloud data could not be acquired and the shoreline position, which is the boundary between land and sea, could not be determined. Not only for the extracted cross-section but at all locations, seafloor topographical data could not be obtained. Various factors likely contributed to this, but ocean conditions appear to have had the greatest influence. A 2017 study by Ozawa et al. (Ozawa, 2017) on airborne laser bathymetry techniques identified major factors attenuating green lasers in water, including scattering by suspended particulate matter, absorption of green lasers by Chromophoric dissolved organic matter (CDOM) dissolved organic matter, reflection of green lasers by whitecaps generated at the water surface, and decreased green laser reflection from low reflectivity seafloor substrates. Among these, whitecap generation can be confirmed visually, and orthorectified aerial imagery in Figure 4 shows more whitecaps during the first survey period compared to the second period. For these reasons, the lack of underwater point cloud data in the first survey is attributed to attenuation from whitecap generation.

In the second survey period, seafloor point cloud data was acquired across most areas from 0 to 6 m depth. Cross-sections show point clouds were obtained up to a maximum depth of 6.3 m, revealing coastal morphology like steps and berms. However, data gaps near shorelines were consistently observed in all cross-sections. These gaps are also largely due to wave effects. Near shorelines, irregular wave patterns make the seawater appear white and turbid, likely causing green laser scattering. Thus, whitecap generation appears to greatly impact measurement capabilities for drone-based green laser surveying in coastal zones. Whitecaps predominantly arise from increasing wind speeds, occurring offshore at around 5 m/s and increasing in frequency with higher wind speeds. Monitoring wind and wave conditions during surveys is therefore critical. Furthermore, all seafloors point cloud analyses hereafter utilize data acquired in the second survey period.

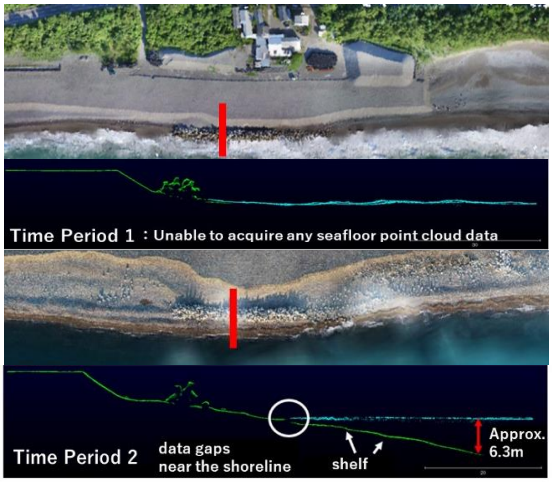

Figure 4. Extraction points and cross section of the first and second period.

3.2.2 3D monitoring of submerged breakwaters: Figure 5 above displays a 3D model created by filtering point cloud data from the second period to remove the data from the sea surface. The 3D model confirms the presence of a submerged breakwater located approximately 125 m offshore with a water depth of about 3 m. Figure 5 below shows an extracted image of the top block of the submerged breakwater and a 3D model of the upper part of the submerged breakwater. By displaying the point cloud data with different colors according to the altitude, a depression of about 50 cm compared to the surrounding area was found in the area enclosed by the red frame. Additionally, the 3D model allows for a qualitative understanding of the movement of the blocks and the state of the depression.

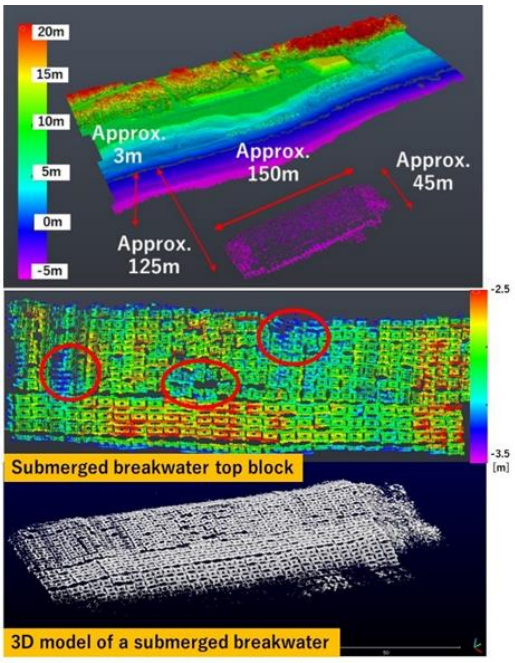

Figure 5. Upper: 3D model with sea level data removed, Lower: Extracted top block of submerged breakwater and 3D model of a submerged breakwater.

3.3 Relationship between Bathymetric Depth and Point Density

3.3.1 Verification Method: As observed in the cross-sectional verification, missing data near the shoreline suggest that the generation of waves, a coast specific phenomenon, significantly influences bathymetric capabilities. This verification aimed to examine the relationship between bathymetric depth obtained through drone surveys and the acquired point density. Figure 6 above illustrates a contour map of the seabed. Point cloud data from the survey were extracted for the seabed and used to create contours. These contours were then divided into 1m areas, and point density was calculated for each area. In this verification, Area A represented depths of 0-1m, Area B 1-2m, Area C 2-3m, Area D 3-4m, Area E 4-5m, and Area F 5-6m. Figure 6 below displays point cloud data for each area. Although there were limited data points beyond 6m in depth, these were excluded from the verification due to insufficient sample size. Additionally, a similar verification was conducted for the landward portion outlined. Point density was defined as the number of point clouds per square meter, as indicated by equation (1).

$$Point\ Density = \frac{Number\ of\ Acquired\ Point\ Clouds}{Area\ (m^2)} \quad (1)$$

In this verification, areas were not calculated separately; instead, the count of point clouds plotted on a unit area cantered around a single point cloud was used as the point density data value. Considering the values provided for each point cloud, their mean, mode, maximum, and minimum values were calculated, and verifications were conducted for each area.

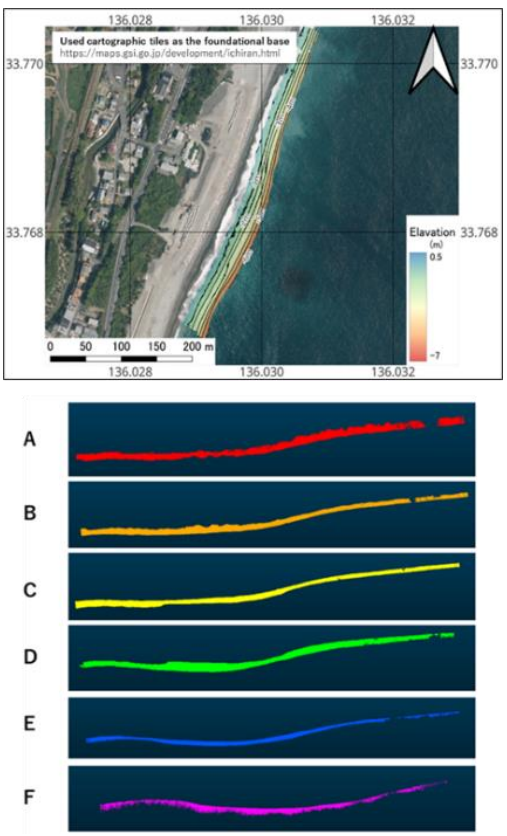

Figure 6. Upper: Contouring of seabed data, Lower: Point cloud data for each area.

3.3.2 Verification Results: Firstly, the calculation of point density in the landward area resulted in 617,593 points cloud data with an average point density of 219.36 points/m^2. The seabed data density calculation results are as follows. Area A: mean 81.51959, mode 63.344; Area B: mean 113.0207, mode 62.389; Area C: mean 172.2026, mode 105.679; Area D: mean 194.0909, mode 177.299; Area E: mean 122.7865, mode 96.766; Area F: mean 61.35358, mode 46.792. Additionally, when the scatter plot of the mean and mode values was graphed, it showed a mountain-shaped scatter distribution. This data will be submitted to an international conference in a scholarly paper. Figure 6 below shows a dot density shaded relief map. Despite significant overall variability, it was noted that, apart from the minimum value, the area with a depth of 3m to 4m (Area D) exhibited the highest values for all parameters, including maximum and mean values. Area C, which displayed the highest mean value and the largest minimum value, showed the most consistent acquisition of point clouds. Comparing areas with depths of 2m and below, such as Area A and B, to Area D, it was evident that both the mean and mode values were lower.

3.4 Extraction of Deformation of Tetrapods by ICP

In this study, we applied the Iterative Closest Points (ICP) algorithm to analyze the data obtained from Shichiri Mihama Beach at two different time periods and extract the changes in the tetrapods. The ICP algorithm performs point cloud matching by iteratively associating scan points and optimizing their positions between the current scan and the reference scan. When applying ICP to extract displacements from a point cloud, rather than matching the entire point cloud, analysis is performed in mesh units of segmented square ranges. Then, the displacement vector is calculated using the average movement amount and direction of the points in each mesh. This mesh size is defined as the mesh size. Also, when matching point clouds for each mesh, the range of point clouds to match needs to be determined. This range is defined as the block range.

Tetrapods can cause coastal erosion and flooding due to subsidence of the sandy ground and movement of the blocks caused by high waves. Currently, visual inspections are conducted to check for subsidence, movement, and damage to the tetrapods. However, it is challenging to accurately assess the overall subsidence amount, and these inspections are time-consuming and pose risks. To improve the efficiency and reduce the labor required for inspections, we conducted this verification to explore the use of drones.

3.5 Alignment and accuracy verification

To prevent systematic errors in the survey from appearing as deformations in point cloud data obtained by drone surveying, five points with no coordinate movement were extracted from the point cloud data obtained over approximately four months, and their positions were adjusted by overlaying them. In Figure 7 above, the points used for the alignment of point clouds are depicted. The green-colored data in this figure represent the data from Period 1, while the red-colored data represent the data from Period 2. The alignment of point clouds involved the extraction of ten points in total, five from each of Periods, including the survey control points used as the reference for adjustment. The coordinates of points 1-5 are shown below. Point 1: Period 1 (x: 2626.3220, y: -247659.6875, z: 8.430985), Period 2 (x: 2626.2729, y: -247659.7344, z: 8.5210), Point 2: Period 1 (x: 2579.1260, y: -247604.4063, z: 11.6994), Period 2 (x: 2579.1411, y: -247604.4375, z: 11.7620), Point 3: Period 1 (x: 2649.2949, y: -247459.6250, z: 13.6860), Period 2 (x: 2649.3330, y: -247459.6250, z: 13.7440), Point 4: Period 1 (x: 2681.9360, y: -247451.3750, z: 11.6869), Period 2 (x: 2682.0029, y: -247451.3594, z: 11.7810), Point 5: Period 1 (x: 2743.48291, y: -247337.9063, z: 5.680), Period 2 (x: 2744.9826, y: -247337.7287, z: 5.7573).

After position adjustment, point clouds of the reference surface (assumed unchanged between the two survey periods) and the wave dissipating block zone to check for anomalies were extracted, and ICP-based anomaly extraction was conducted simultaneously. Three surfaces were extracted for the reference surface: 1) roof of house 1, 2) roof of house 2, and 3) road surface. Figure 7 below shows the extracted surfaces. For verification, anomalies were extracted with a mesh size of 1. The ICP anomaly extraction results were an average of 0.032 m for 1) roof of house 1, 0.046 m for 2) roof of house 2, and 0.049 m for 3) road surface. Since no particular trend was observed in the anomaly directions, it is considered that systematic errors causing point cloud deviation were eliminated. Given that the average anomaly for the assumed unchanged surfaces between the two periods was 0.044 m, for this verification, anomalies below 0.05 m are considered permissible errors. When ICP extracts anomalies 0.05 m or greater, they will be regarded as true anomalies.

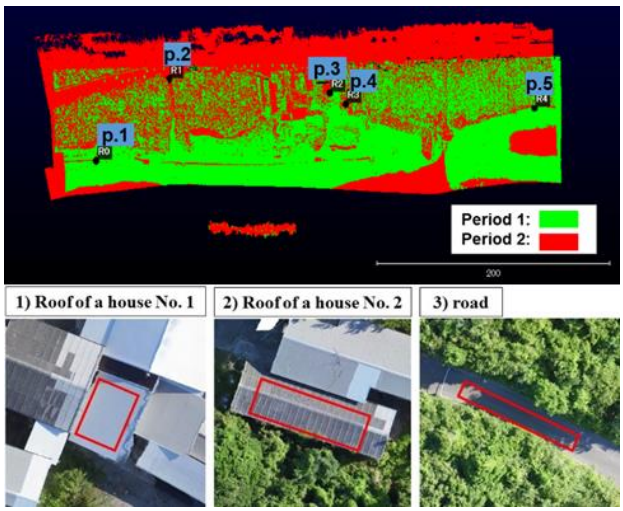

Figure 7. Upper: The points utilized for point cloud registration, Lower: Surface used for accuracy verification.

3.6 Results of the deformation extraction of vanishing wave blocks (tetrapod)

3.6.1 Overall deformity: Upper Figure 8 shows an orthographic image from above (first period) and lower shows the overall deformation of the breakwater viewed offshore obtained by ICP. As a result of the deformation extraction, an overall subsidence of 33.8 cm was confirmed, and it was found that only the area surrounded by red showed a larger deformation compared to the surrounding area, with a deformation amount of 118.3 cm. Furthermore, since the direction of this deformation is pointing significantly diagonally downward to the right, it is considered that there was movement in the surrounding blocks that showed deformation, rather than a part of the overall subsidence.

3.6.2 Localized deformity: The second figure from the top in Figure8 illustrates the variation in the quantity of wave dissipating blocks, marked with color. It is evident, as previously mentioned, that the area enclosed within the red boundary exhibits notably larger changes compared to the surrounding blocks. The second figure from the bottom in Figure8 displays an extraction of the blocks in the vicinity that demonstrated substantial changes, highlighting that only the blocks within the red boundary show significant variation. This implies that these specific blocks are not subsiding but rather relocating, indicating the capability of identifying the displaced blocks using drone surveys and ICP (Iterative Closest Point). Furthermore, Figure 8 below represents an orthoimage of the targeted blocks. Although it is an orthoimage constructed by overlaying multiple aerial photographs, it enables the observation of changes over two different time periods.

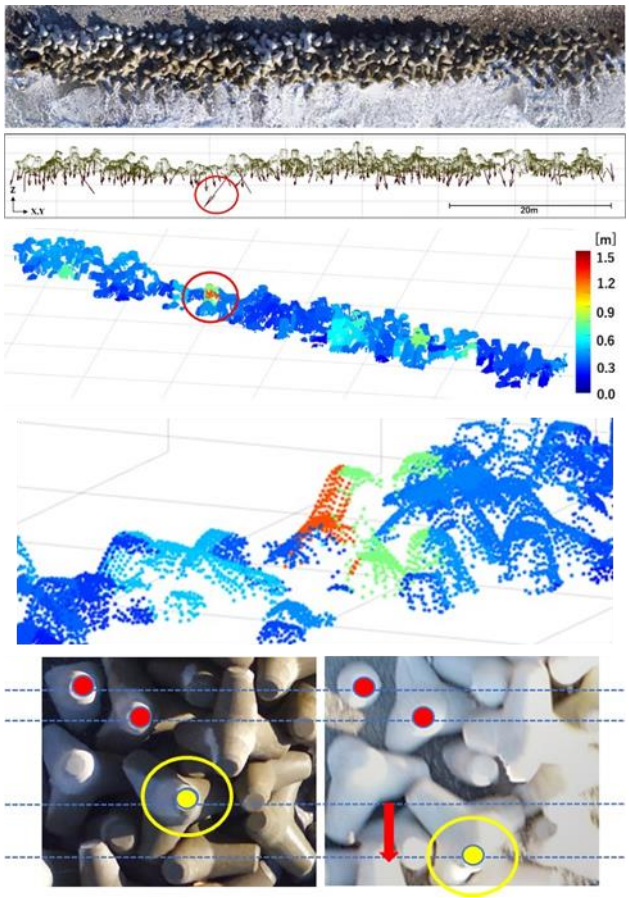

Figure 8. Orthographic image and the overall deformation of the breakwater viewed offshore obtained by ICP, Overall deformation amount step colour chart, The extracted blocks and Orthoimage of moving block.

4. DISCUSSION, CONCLUSIONS AND FUTURE ISSUES

In this study, we attempted coastal area monitoring using drone surveys as a novel methodology, aiming to understand the basic performance and extract changes in wave dissipation blocks. Analysis through cross-sectional diagrams enabled the acquisition of point cloud data up to a maximum of 6.3 meters, allowing us to confirm the obtained coastal terrain, including features such as steps. However, notable data gaps were observed near the coastline, exhibiting significant variations based on the survey periods. During the initial period, not only the extracted cross-sections but also various locations failed to acquire seabed terrain data. Several factors could contribute to this issue; however, we believe that oceanic conditions exert the most significant influence. Research by Ozawa et al. (Ozawa, 2017) on airborne laser bathymetry highlighted factors significantly attenuating green lasers, including scattering due to suspended matter in water, absorption by dissolved organic matter in water, reflection caused by whitecaps formed on the water surface, and reduced reflection from low-reflective substances at the water bottom. Particularly, the occurrence of whitecaps could be visually confirmed, with ortho-images captured from above (Figure 4) indicating more frequent whitecap occurrences in the initial period compared to the subsequent one. Consequently, we attribute the inability to acquire underwater point cloud data during the initial survey to whitecap occurrence. Similar data gaps near the shoreline were observed in measurements during the subsequent period, suggesting a significant influence of waves. The irregular state of waves near the shoreline causes seawater to become turbid, thus contributing to scattering of green. Thus, we argue that whitecap occurrence significantly affects the measurement capabilities of drone-based green laser surveys in coastal regions. Whitecap occurrence is primarily associated with increased wind speeds. It is known to occur when offshore wind speeds reach approximately 5m/s, increasing in frequency with higher wind speeds. Therefore, understanding wind speed and wave conditions is deemed crucial during surveys.

In the three-dimensional model of submerged breakwaters, it was possible to qualitatively confirm block movements and depressions at a glance. Particularly, submerged breakwaters, characterized by their submerged-type structures where the tops are lower than the water surface, are not easily assessable in terms of height or similar metrics from land, unlike onshore structures or offshore breakwaters (Hamaguchi, 2018). Conventional monitoring methods struggle to capture the shape of extensive shallow structures with high density. It is believed that using drones could enable more efficient monitoring of such structures in shallow areas.

Submerged breakwaters have the advantage of attenuating wave energy by inducing wave breaking at their crests, yet this leads to an increase in the average water level due to the resultant breaking waves. Consequently, a flow is induced towards the opening from the submerged breakwater, causing scouring of the seabed behind the breakwater due to this flow (Japan Port Consultants Association, 2021). Especially when placing submerged breakwaters close to the shore, the resulting scouring may impact changes in the terrain near the shoreline. Therefore, it is believed that comprehensive monitoring of coastal erosion can be achieved by acquiring not only structural information but also three-dimensional point cloud data of the seabed simultaneously through drone surveys, enabling the assessment of both the condition of the submerged breakwaters and the scouring state of the seabed caused by these structures.

In the verification of survey depth and point density, it was observed that the average point density reached its maximum within the depth range of 3 to 4 meters, while there was a declining trend in point density in shallower areas. Typically, in underwater environments, it is expected that as water depth decreases, point density would increase due to the attenuation of green lasers. However, in this validation, contrary to expectations, coast-specific phenomena such as the disturbance of whitecaps and bottom sediment are believed to have led to deteriorating water quality. Regarding Areas E and F, the decrease in point density is considered to have occurred due to the attenuation of green lasers caused by increased water depth. The absence of data and the reduced point density in shallow water areas are thought

to result from coast-specific occurrences of whitecap formation and the stirring of seafloor sand due to wave action, leading to decreased water transparency.

In addition, the extraction of changes in the wave dissipation blocks by ICP revealed an average subsidence of the entire wave dissipation block by 33.8 cm, and an approximate movement of local blocks by around 118 cm. Notably, in Mie Prefecture, where Shichiri Mihama Beach is situated, record-breaking heavy rainfall exceeding 120 mm per hour was observed in August and October of 2021. There exists a high likelihood that the breakwater experienced deformations such as subsidence or displacement between the first and second measurement periods due to these extreme weather events. Moreover, in locations like Shichiri Mihama Beach, where there is no reference plane in the vicinity, visually capturing the overall subsidence is extremely challenging. Determining subsidence by assessing height from the ground is typically utilized in cases where there is no reference plane, but due to substantial erosion in the surrounding area, visual inspection alone does not facilitate comprehensive understanding of the overall subsidence. Therefore, the extraction of three-dimensional deformation via drone surveys can be regarded as a viable future monitoring method for structures, given the limitations of visual inspection. Additionally, the results from the overall change extraction through ICP enabled identification of specific areas with potential localized movement, allowing focused examination on those sections for the identification of shifted blocks. Consequently, this screening method can be used to identify blocks with changes during routine inspections or emergency checks post-disaster, aiding in detecting significant alterations. Particularly, conducting inspections immediately after a disaster poses risks; hence, the application of this method to underwater structures could prove highly beneficial in the future. However, while ICP can verify changes and movements by associating point clouds, further verification is required to ascertain whether damages to wave dissipation blocks with complex structures can be accurately identified through ICP.

Drones have the capability to acquire higher-density point clouds compared to Airborne Laser Bathymetry (ALB), offering potential in understanding the subsidence conditions and anomalies in complex-shaped wave dissipation blocks. Moving forward, it is essential to establish the fundamental performance through data acquisition under various conditions. Additionally, it is imperative to verify the accuracy of change extraction in coastal areas using Iterative Closest Point (ICP) under conditions where accurate change quantities are known.

ACKNOWLEDGEMENTS

At the end, I deeply appreciate the support and assistance provided by many individuals in the completion of this paper. In particular, I am sincerely grateful to Professor Nishiyama of the Graduate School of Environmental and Life Science Program at Okayama University for his continuous and enthusiastic guidance.

REFERENCES

Hirayama, H., Tsujimoto, G., Shimada, F., Honda, N., 2017. Coastal Engineering, Corona Press, 6-7.

Japan Port Consultants Association., 2021: *Port Engineering*, Asakura Publishing, 195-196.

Ministry of Land, Infrastructure, Transport and Tourism, 2015. Situation Changes Related to the National Land in 2050 Interim Summary on Beach Conservation.

Ministry of Land, Infrastructure, Transport and Tourism, 2019. Current Status of Efforts for Coastal Conservation Document 2.

Ministry of Land, Infrastructure, Transport and Tourism, Directions for the Impact of Climate Change and Adaptation in Coastal Areas.

Tomii, T., 2021. Utilization of Drone-mounted Green Lasers, Reprint Measurement and Control, Vol. 60, No. 10.

Ministry of Land, Infrastructure, Transport and Tourism, 2020. Promotion of Digital Transformation (DX) at the Ministry of Land, Infrastructure, Transport and Tourism.

Ministry of Land, Infrastructure, Transport and Tourism, 2016. Promotion of i-Construction, Document 1.

Ikeda, S., Fujiyama, T., Monowaki, K., Yokota, T., Watanabe, T., Kuronuma, N., Tsukamoto Y., 2019. Survey of Rumoi Coast in Hokkaido using Green Laser, Journal of JSCE B2 (Coastal Engineering), Vol. 72, No. 2.

Huong, V.T.L., Kiku, M., Nishinora, Y., Nakamura, T., Mizutani, N., 2015. Study on Coastal Morphological Changes in Shichiri Mihama Ida Coast, Journal of JSCE B2 (Coastal Engineering), Vol. 71, No. 2.

Ozawa, J., Okabe, T., Kawamura, H., Miyazaku, T., Tachibana, K., 2017. Airborne Laser Bathymetry Technology, Photogrammetry and Remote Sensing, Vol. 56, No. 6.

Hamaguchi, K., Katou, F., Hashimoto, K., Koganezawa, T., 2018. Study on Correction Method for Refraction Effects at Sea Surface in Understanding the Shape of Artificial Reefs using UAVs, Journal of JSCE B2 (Coastal Engineering), Vol. 74, No. 2.

Rural Development Bureau, Ministry of Agriculture, Forestry and Fisheries, Fisheries Agency Disaster Prevention Section, Ministry of Land, Infrastructure, Transport and Tourism Water Management and Land Conservation Bureau Coastal Division, Ministry of Land, Infrastructure, Transport and Tourism Ports and Harbors Bureau, 2014. Coastal Conservation Facility Maintenance Manual.

Ports and Harbors Bureau, Ministry of Land, Infrastructure, Transport and Tourism, 2021. Guidelines for Inspection and Diagnosis of Port Facilities, 2-11.

Tomonai, M., 2018. Introduction to SLAM: Technology for Robot Self-Localization and Map Construction, Omusha Publishing.

Yamanoi, K., Yabuki, T., Esaki, T., 2021. Application of drone photogrammetry for inspection of breakwater armour units. Coastal Engineering Journal, 63(2), 142-157.

Mancini, F., Dubbini, M., Gattelli, M., Stecchi, F., Fabbri, S., Gabbianelli, G., 2013. Using unmanned aerial vehicles (UAV) for high-resolution reconstruction of topography: The structure from motion approach on coastal environments. Remote Sensing, 5(12), 6880-6898.

Casella, E., Rovere, A., Pedroncini, A., Stark, C.P., Casella, M., Ferrari, M., Firpo, M., 2016. Drones as tools for monitoring beach topography changes in the Ligurian Sea (NW Mediterranean). Geo-Marine Letters, 36(2), 151-163.

Laporte-Fauret, Q., Marieu, V., Castelle, B., Michalet, R., Bujan, S., Rosebery, D., 2019. Low-Cost UAV for high-resolution and large-scale coastal dune change monitoring using photogrammetry. Journal of Marine Science and Engineering, 7(3), 63.

Scarborough, J., Roelvink, D., Jaffe, B., Cowell, P., 2019. Mapping coastal erosion hazard zones using machine learning of pretrained CNNs and satellite imagery. Coastal Engineering, 150, 175-186.